Published in final edited form as:
Nat Cell Biol. ; 14(4): 416–423. doi:10.1038/ncb2446.

Single-molecule assays reveal that RNA localization signals regulate dynein-dynactin copy number on individual transcript cargoes

Mamta Amrute-Nayak[1] and **Simon L. Bullock**[1,2]
[1]Cell Biology Division, MRC Laboratory of Molecular Biology, Hills Road, Cambridge, CB2 0QH, UK

Abstract

Subcellular localization of mRNAs by cytoskeletal motors plays critical roles in the spatial control of protein function[1]. However, optical limitations of studying mRNA transport *in vivo* mean that there is little mechanistic insight into how transcripts are packaged and linked to motors, and how the movement of mRNA:motor complexes on the cytoskeleton is orchestrated. Here, we have reconstituted transport of mRNPs containing specific RNAs *in vitro*. We show directly that mRNAs that are either apically localized or non-localized in *Drosophila* embryos associate with the dynein motor and move bidirectionally on individual microtubules, with localizing mRNPs exhibiting a strong minus-end-directed bias. Single-molecule fluorescence measurements reveal that RNA localization signals increase the average number of dynein and dynactin components recruited to individual mRNPs. We find that, surprisingly, individual RNA molecules are present in motile mRNPs *in vitro* and present evidence that this is also the case *in vivo*. Thus, RNA oligomerization is not obligatory for transport. Our findings lead to a model in which RNA localization signals produce highly polarized distributions of transcript populations through modest changes in motor copy number on single mRNA molecules.

A valuable model for studying mRNA transport is the *Drosophila* syncytial blastoderm embryo. Here, cytoplasmic dynein, the minus-end-directed microtubule motor, and its accessory complex dynactin are required to translocate a subset of mRNAs to the apical cytoplasm[2]. This is consistent with the overall enrichment of microtubule minus-ends apically, with plus-ends extending basally[3]. Apical transport is also dependent on the RNA binding factor Egalitarian (Egl) and its partner Bicaudal-D (BicD)[4-6]. This protein complex binds directly both to components of the dynein-dynactin complex[5, 7] and RNA localization signals[4], specialized stem-loops that mediate asymmetric transcript enrichment.

Following injection into embryos, fluorescent, *in vitro* synthesized transcripts assemble into mRNPs that move bidirectionally[8, 9]. Net apical accumulation of localizing RNAs is due to longer uninterrupted movements, on average, in the apical direction than in the basal direction[8, 9]. Surprisingly, RNAs that have a uniform distribution endogenously also move bidirectionally upon injection, but with little net bias[8]. This observation contributed to the speculative model that Egl, BicD and RNA signals are not obligatory for linking mRNAs to motor complexes, but drive apical localization by increasing the frequency of dynein-driven movements of a generic bidirectional transport complex[8]. However, it was unclear if

---

[2]Correspondence should be addressed to (sbullock@mrc-lmb.cam.ac.uk) .

Contributions MA and SB conceived the project. MA developed the *in vitro* assays, performed all *in vitro* experiments and analyzed the data. SB performed the embryo injections and *in situ* hybridizations and analyzed the data. MA and SB interpreted the data. SB and MA wrote and edited the manuscript, respectively.

Europe PMC Funders Author Manuscripts

reversals of mRNPs in the apical-basal axis represent movements on single microtubules or switching between mixed polarity filaments, and what mechanism is used by RNA localization signals, Egl and BicD to impart a net minus-end-directed bias to transport.

To explore the basis of differential mRNA sorting we set out to reconstitute transport *in vitro* of isolated RNPs carrying either a well-characterized, apically localizing RNA, *fs(1)K10* (*K10*), or a mutant in which the 44 nucleotide localization signal[6, 10] had been destroyed in the context of an otherwise wild-type *K10* transcript ($K10^{mut}$). This mutation prevents enrichment of the injected RNA apically (Ref.11 and Supplementary Fig. S1) by substantially diminishing the net minus-end bias to bidirectional transport (Supplementary Table S1).

In vitro synthesized *K10* or $K10^{mut}$ RNAs—body-labelled with multiple Cy3-UTPs—were incubated with *Drosophila* embryonic extracts in the presence of biotinylated microtubules and streptavidin-conjugated magnetic beads (Fig. 1a). Motor proteins and their associated complexes were then captured from extracts based on their affinity for the exogenous microtubules, followed by brief washing and release with ATP. The released fraction included known constituents of RNA:motor complexes (Fig. 1b), but still represented a complex mixture of many proteins (data not shown).

This fraction was added to an imaging chamber and viewed with total internal reflection (TIRF) microscopy. Typically five to ten puncta of Cy3-labelled *K10* or $K10^{mut}$ RNA exhibited persistent movements along fluorescein-labelled microtubules preadsorbed on the coverslip (Fig. 1c–e; Supplementary Movies S1–S3;), with speeds of up to 1.5 $\mu m\ s^{-1}$ (Supplementary Fig. S2a). These presumably represented active RNA:motor complexes assembled in the extract.

Approximately half of the motile *K10* and $K10^{mut}$ mRNPs underwent at least one reversal in the direction of movement along individual microtubules before the Cy3 signal was lost (Fig. 1d,e; Supplementary Movies S1–S3). Mean square displacement analysis indicated that active transport contributed to the movement of even the most oscillatory mRNPs (Supplementary Fig. S2b). Consistent with a physiological role for motors in transporting non-localizing mRNAs, we observed $K10^{mut}$ RNA's association with dynein, and transport, when RNA:motor complexes were assembled and washed in 150 mM salt (Supplementary Fig. S2c,d), not just the 50 mM concentration used in all other motility assays. Collectively, these data demonstrate that both localizing and non-localizing mRNPs are capable of bidirectional transport on individual microtubules.

We next quantified the motile properties of localizing and non-localizing mRNPs by performing *in vitro* motility assays on polarity-marked microtubules (Supplementary Movie S4). *K10* mRNPs exhibited a strong net minus-end bias in their transport, whereas $K10^{mut}$ mRNPs did not (Fig. 2a). Net transport of *K10* mRNPs was associated with substantially longer runs in the minus-end direction than in the plus-end direction (Fig. 2b). Run lengths of $K10^{mut}$ mRNPs also had a minus-end bias, but the magnitude of the difference was much lower than for *K10* RNAs (Fig. 2c). Qualitatively, these findings are reminiscent of the ability of the *K10* localization signal to significantly augment apical and basal run lengths *in vivo*, with much stronger effects on apical travel distances (Supplementary Table S1).

The association time of Cy3 signals with microtubules was similar for motile *K10* and $K10^{mut}$ mRNPs (Fig. 2d). Thus, measured differences in net motion of the two RNAs were not due to decreased dissociation of localizing RNPs from microtubules. Rather the localization signal must enhance the ability of an mRNP to move persistently in the minus-end direction before reversing. Consistent with this notion, the frequency of reversals was significantly lower for *K10* than for $K10^{mut}$ mRNPs (Fig. 2e).

We also monitored the *in vitro* behaviour of the *h* RNA, which localizes apically in the embryo[12], and the *Kr* transcript, which has a uniform apical-basal distribution[8] (Fig. 2f–h and Supplementary Fig. S2b). Reminiscent of the behaviour of each injected mRNA in embryos (Ref. 8 and Supplementary Table S1), both mRNP species underwent bidirectional transport *in vitro*, with those containing *h* RNA exhibiting significantly greater net minus-end-directed motion than those containing *Kr* (Fig. 2f–h).

Our findings provide direct evidence for the previous model that localizing and non-localizing mRNAs undergo differential transport on individual microtubules, with localizing RNAs accumulating apically in embryos because RNA signals increase the probability of minus-end-directed motion of a bidirectional transport complex[8]. It is plausible that the extent of association of non-localizing mRNPs with motors is exaggerated in our assay by the presence of a microtubule affinity purification step. Nonetheless, a physiological interaction between uniformly distributed RNAs and motors is supported by our previous observation that the spreading of endogenous *Kr* RNA in the blastoderm cytoplasm is dependent on dynein[8]. Transport of non-localizing mRNPs presumably facilitates intermolecular interactions in the crowded cytoplasm[13].

We next investigated the mechanism by which localization signals increase the frequency of minus-end-directed motion. It is possible that dynein needs to dissociate from mRNPs in order for them to undergo plus-end-directed motion, with localization signals driving net minus-end movement by reducing the rate with which this happens. However, this scenario is highly unlikely because GFP::Dynein light intermediate chain (Dlic) was detected with Cy3-labelled mRNPs during movements in both directions along microtubules *in vitro* (Supplementary Fig. S2e).

We previously speculated that localization signals, through Egl and BicD, mediate net minus-end-directed transport by recruiting additional dynein motors to those present on non-localizing mRNPs[8]. Direct evidence for such a model was lacking, however, as it is not possible to visualize motor components on mRNPs *in vivo*. More recent work on lipid droplet motion in *Drosophila* embryos—which also involves BicD[14]—has provided evidence that regulation of absolute motor copy number is not significant for the control of bidirectional transport properties[15]. Thus, it was possible that dynein number is the same on localizing and non-localizing mRNPs, with differential sorting due to regulation of the activity of the motors.

To investigate this issue we employed stepwise photobleaching to assess the relative copy number of motor components associated with *K10* or *K10^{mut}* RNPs *in vitro* (Fig. 3 and Supplementary Fig. S3a,b). This method allows the number of fluorescent molecules in individual complexes to be estimated by counting the number of discrete step changes in fluorescence intensity during photobleaching[16-20]. The ability of our photobleaching assay to estimate the copy number of fluorescent molecules was supported by predominantly two-step photobleaching of microtubule-associated puncta of a GFP-tagged tailless kinesin-1 motor (Supplementary Fig. S3c), which is predicted to form a dimer[16, 21].

Motor complexes were captured from extracts of transgenic embryos expressing GFP-tagged versions of either the dynactin subunit Dynamitin (Dmn) or Dlic in the presence of Cy3-labelled *K10* or *K10^{mut}* RNAs. Long-term photobleaching, performed on RNA:motor complexes immobilized on microtubules in the no nucleotide state, revealed variation in the number of GFP bleaching steps per complex (Fig. 3a-d). This was expected because the multiple molecules of Dlic and Dmn present in each dynein-dynactin complex will represent mixtures of GFP-tagged and endogenous Dlic and Dmn (Supplementary Fig. S3d).

The mean number of decay steps of GFP::Dlic and GFP::Dmn was, respectively, ~70% and ~55% greater on *K10* mRNPs than on $K10^{mut}$ mRNPs (Fig. 3c-e; $p < 0.001$). These data provide direct evidence that localization signals increase the average copy number of dynein-dynactin complexes per mRNP. Consistent with this notion, when *K10* and $K10^{mut}$ RNAs were immobilized via an aptamer to an affinity matrix and incubated with embryonic extracts, we observed greater recruitment of Dlic to the population of localizing RNA (Supplementary Fig. S3e).

We next combined the photobleaching data with quantification of the ratios of GFP-labelled to unlabelled Dlic and Dmn in the material injected into the imaging chamber (Supplementary Fig. S3d), and published data on the stoichiometry of Dlic and Dmn per motor complex (Supplemental Fig. S3d legend). This analysis indicated that there is a low number of dynein-dynactin complexes on captured non-localizing mRNPs (most likely an average of one or two copies per mRNP), with localization signals increasing the proportion of mRNPs in the population that have recruited additional copies of this complex. Long-term experiments, involving significant technological advances, will be needed to determine with absolute precision the copy number of dynein and dynactin within motile RNA:motor complexes.

There are large increases in the duration of minus-end-directed runs when two versus one, or three versus two, dynein motors are active on a bead[22]. By increasing the likelihood of engaging in minus-end- versus plus-end-directed motion, recruitment of additional dynein-dynactin complexes is therefore likely to play an important role in generating the overall directional bias exhibited by the population of localizing mRNPs. The *in vivo* significance of dynein copy number for controlling mRNP motility is supported by our earlier observations that increasing the concentration of Dynein light chain—which links cargoes to the motor complex—augments minus-end motion of mRNPs in a perduring fashion and leads to weak apical enrichment of endogenous *Kr* RNA[8]. Nonetheless, we cannot rule out the possibility that an RNA localization signal, through Egl and BicD, also enhances minus-end-directed transport by increasing the activity of the additional dynein-dynactin it recruits, or even by promoting its co-ordination with other motor complexes on the mRNP. This latter scenario could explain the increases in plus-end run lengths observed for localizing versus non-localizing RNA populations (Figure 2b, c, g and h; Supplementary Table S1).

Work on other mRNA targeting systems has provided evidence that individual localizing mRNPs can contain multiple RNA molecules[23-26], with intermolecular RNA:RNA interactions obligatory for asymmetric localization in at least one case[27]. We therefore investigated *in vitro* if localizing mRNPs recruit more dynein-dynactin copies than non-localizing mRNPs because they contain more RNA molecules. We produced *K10* or $K10^{mut}$ RNAs body-labelled with Cy3 and determined the mean number of dyes per transcript. Following assembly of mRNPs on these RNA preparations, stepwise photobleaching was used to count the number of Cy3 decay steps within individual microtubule-associated motor complexes (Fig. 4a and Supplementary Fig. S4). Surprisingly, the mean numbers of Cy3 decay steps observed for *K10* or $K10^{mut}$ mRNPs fit best with a single RNA molecule being present in the majority of complexes (Fig. 4a). Almost exclusive one-step photobleaching of *K10* mRNPs contain RNA labelled at the 3′ end with a single Cy3 also supports this notion (Fig. 4b), as does our finding that when Alexa 488-labelled preparations of a localizing RNA were mixed with Cy3-labelled preparations of the same RNA we never observed motile mRNPs containing both fluorophores (Fig. 4c-e). These experiments demonstrate that localization signals increase the average copy number of dynein-dynactin complexes recruited to individual RNA molecules and that RNA multimerization is not obligatory for motility or directional transport.

We next used a non-enzymatic *in situ* hybridization technique capable of detecting single RNA molecules in *Drosophila* embryos[28] to investigate whether an individual copy of an RNA species is present in localizing mRNPs *in vivo*. We focused on the *h* mRNA which, unlike *K10*, is abundantly expressed in the blastoderm. Embryos were hybridized simultaneously with two antisense probes against the same sequence in *h*, which were labelled with different haptens and detected with antibodies conjugated to different fluorophores (Fig. 5a–e). Co-localization of cytoplasmic signals from these competitive probes was only detected rarely both apically (Fig. 5c–e and o) and in more basal regions (Supplementary Fig. S5a,b). Overlap of signals from these probes could, however, be detected at the sites of nascent transcription in the nuclei (Figure 5n), where multiple copies of the same transcript accumulate[29].

To test whether the relatively low degree of co-localization of the competitive probe signals in the cytoplasm was significant we simulated a random distribution of dots by rotating the image of the signal derived from one of the probes in the apical cytoplasm by 90° and overlaying it on the original orientation of the image derived from the other probe[28]. Very similar proportions of dual-coloured puncta were observed in the rotated and original configurations (Fig. 5o), indicating that the co-localization was attributable to chance overlap of the signals. The incidence of immediately adjacent, but not co-localized, signals from the competitive probes was also the same in the rotated and original configurations (Supplementary Fig. S5c), arguing against the existence of very large mRNPs containing multiple copies of *h* that can be clearly resolved.

In contrast, we frequently detected co-localization of two probes to non-overlapping regions of *h* in the apical cytoplasm (Fig. 5a, g–i and o), as well as more basally (Supplementary Fig. S5a,b). This method can therefore unambiguously detect two target sites within the same cytoplasmic mRNP, should they exist. Failure to detect simultaneous hybridization of two probes targeted to the same sequence therefore indicates that individual copies of *h* RNA are present in the vast majority of localizing mRNPs.

We also did not detect significant cytoplasmic co-localization of *h* and *even-skipped* (*eve*) (Fig. 5k–m and o), another apically localized pair-rule mRNA that is expressed abundantly in blastoderm embryos in a pattern that overlaps partially with that of *h* (Ref. 30 and Fig. 5j). Although we cannot rule out the possibility that *h* RNA molecules are packaged into mRNPs with other localizing RNA species, this result provides evidence that apically localizing mRNPs *in vivo* contain a single RNA molecule. Assembling many transcript molecules into a single mRNP might intuitively seem a more efficient strategy for translocating an mRNA population. However, such a mechanism would present an additional challenge in so far as localizing and non-localizing RNA species would need to be packaged independently. Indeed, the long-standing notion than neuronal RNA transport complexes contain large numbers of transcripts has been challenged recently[31].

In summary, we have reconstituted transport of specific mRNA species along individual microtubules *in vitro* and employed single molecule resolution measurements to shed light on the composition of transport complexes. An *in vivo* study of *oskar* mRNA transport in *Drosophila* oocytes has demonstrated that asymmetric RNA localization can be achieved by a random walk of a single motor species along a weakly polarized microtubule cytoskeleton[32]. Our findings provide direct evidence for an additional mechanism for RNA targeting in which localization signals control sorting by regulating the net directionality of bidirectional motor complexes on individual microtubules. We propose that this is associated with modest differences in the number of motors assembled on individual mRNA molecules. Our findings raise fascinating questions about how dynein-dynactin and the unidentified plus-end motor(s)[9] are bound to localizing and non-localizing mRNA molecules and how their activities are orchestrated in time and space.

Methods

Drosophila strains

Wild-type embryos were of the OR-R strain. *P(mat-tub-α4-taillessKhc::GFP (1-849))* (Ref. 34), *P(Ubi-GFP::DLIC)* (Ref. 35) and *P(mat-tub-α4-GFP::Dmn)*(Ref. 36) lead to ubiquitous expression of the GFP fusion proteins during early development and were kind gifts of Isabel Palacios, Jordan Raff and Antoine Guichet, respectively.

Fluorescent RNA synthesis and injection

Capped RNA was synthesized as described previously, using T7- or T3- mediated transcription[8]. For *in vitro* and *in vivo* RNA motility assays, a 1:3 ratio of fluorescent UTP (Alexa488-UTP (Invitrogen) or Cy3-UTP (PerkinElmer):unlabelled UTP was used in the reaction, typically resulting in an average of ~4 fluorophores per 1000 nt of RNA. For photobleaching experiments either a ratio of 1:39 Cy3-UTP to unlabelled UTP was used, resulting in an average of ~ 0.4 fluorophores per 1000 nt, or, following transcription, non-fluorescent RNAs were labelled at the 3′end with a single dye using pCU-Cy3 (a kind gift of Eric Miska), as described[37].

Wild type *K10* RNA and $K10^{mut}$ RNA were as described previously[11], and corresponded to the entire 1432-bp 3′UTR and an 860-bp portion of the 3′ genomic sequences. $K10^{mut}$ was referred to as $K10^{scrambled}$ in ref. 11, and has the constituent bases of the apical localization signal randomized. *h* and *Kr* RNAs corresponded to the full length cDNAs (~1900- and ~2300-bp, respectively). Injection of embryos with fluorescent RNA followed by time-lapse imaging and automatic particle tracking was as described[8].

Microtubule polymerization and adsorption to glass

Tubulin monomers, of porcine or bovine origin, (Cytoskeleton Inc.) were polymerized according to the manufacturer's instructions. Biotinylated microtubules for capturing motors were polymerized using a 1:10 ratio of biotinylated-tubulin to tubulin for 5 min. Fluorescein-labelled microtubules were polymerized using a 1:25 ratio of fluorescein-tubulin to tubulin for 15 min. Polarity-marked microtubules were produced by first allowing polymerization of a 1:5 ratio of fluorescein-tubulin to tubulin for 5 min. Unlabelled tubulin was then added to the mixture to dilute the fluorescent-tubulin to a 1:50 ratio and the mixture incubated for a further 15 min, during which time predominant elongation in the plus-end direction resulted in a relatively bright minus-end segment. Minus-end labelling with this method was confirmed with microtubule gliding assays using purified mammalian dynein-dynactin complexes (kindly provided by Andrew Carter). Microtubules labelled with both Cy5 and biotin were polymerized with a 1:10:25 ratio of Cy5-tubulin, biotinylated-tubulin and unlabelled tubulin for 15 min. Following polymerization, microtubules were diluted in PEM polymerization buffer (Cytoskeleton Inc.) containing taxol to a final concentration of 20 μM. Unincorporated tubulins were removed by ultracentrifugation in a 60% glycerol cushion buffer.

Microtubules were adsorbed to the coverslip in a flow cell in one of two ways, with indistinguishable results in RNA motility assays: they were either allowed to associate non-specifically with the glass or they were associated through a biotin-streptavidin-biotin linkage[38] (using microtubules labelled with both fluorescein and biotin). Washes with PEM buffer containing 20 μm taxol were used to remove unbound microtubules after 5 min, followed by blocking of non-specific binding sites on the glass surface with 0.5 mg ml^{-1} bovine serum albumin (BSA).

In vitro RNA motility assay

Extracts were produced from 0 – 6 h embryos by homogenizing in DXB buffer (30 mM Hepes pH 7.3, 50 mM KCl, 2.5 mM $MgCl_2$, 250 mM sucrose, 5 mM DTT, 10 μM MgATP and 2 x Complete (EDTA-free) protease inhibitors (Roche)) as described[8] using 4 ml of buffer per g of embryos. Typically the supernatant derived from 50 mg of embryos was mixed with 100 ng of *in vitro* transcribed fluorescently-labelled mRNA and 50 μg biotinylated microtubules. This mixture was agitated for 5 min at room temperature (RT) to allow recruitment of motor complexes to the fluorescent RNA. Cargo:motor complexes bound to biotinylated microtubules were captured by incubation with 350 μg of streptavidin coated magnetic beads (Bang Laboratories) for a further 5 min at RT. Magnetic beads were washed 3 – 4 times in DXB buffer, followed by elution of cargo:motor complexes from the microtubules by incubation for 2 min in assay buffer (AB: 30 mM HEPES-NaOH, 5 mM $MgSO_4$, 1 mM EGTA, 1 mM DTT and 0.5 mg ml^{-1} 4 BSA) containing 4mM MgATP.

The released fraction was introduced together with antibleach system (0.5 μg ml^{-1} glucose oxidase, 470 units ml^{-1} of catalase, 10 mM DTT and 15 mg ml^{-1} glucose) into a flow chamber with fluorescein-labelled microtubules preadsorbed to the coverslip. Microtubules and Cy3-labelled RNA molecules were visualized at RT with a TIRF microscope (Olympus) equipped with a 100x objective (PlanApo, 1.45 NA TIRFM). Images of microtubules and RNAs were acquired sequentially with a 300 ms exposure time for each channel, using an iXon EM+ DU-897 camera (Andor). The movement of mRNPs on polarity-marked microtubules was analyzed using kymographs generated in ImageJ.

For the experiments in figure 4c–e, 100 ng each of Alexa488-labelled *K10* and Cy3-labelled *K10* or 100 ng each of Alexa488-labelled *h* and Cy3-labelled *h* RNA were added to the embryo extract before capturing motor complexes on microtubules and releasing them into a flow cell containing Cy5-labelled microtubules. Images of microtubules were captured at the beginning and end of a series of alternating images of the Alexa488 and Cy3 signals.

RNA affinity purifications

Uncapped RNAs were transcribed from the pTRAPv5 vector (Cytostore Inc.), resulting in the incorporation of two 5′ copies of the S1 streptavidin binding aptamer. RNAs were tethered to streptavidin magnetic beads (Invitrogen) and affinity purifications from embryo extracts, including elution of RNA:protein complexes with biotin, performed as described[4, 8]. Aptamer-linked *K10* and $K10^{mut}$ RNAs were ~ 1200 nt long and contained the majority of the 3′UTR; our preliminary studies indicated that substantially longer RNAs are not efficiently coupled to beads.

Stepwise photobleaching

Cy5-microtubules were bound to the coverslip in the flow chamber using a biotin-streptavidin-biotin link as described above. Motor complexes, captured from extracts from transgenic embryos in the presence of Cy3-RNAs, were released from the biotinylated microtubules with 2 mM MgATP. 2 mM MgADP was added to the released fraction just prior to its addition to the flow cell to promote binding of the motor complexes to microtubules.

After a 5 min incubation of cargo-motor complexes with the microtubules, unbound complexes were washed off with AB solution containing a 10-fold lower concentration of antibleach system than used in the motility assay and no nucleotide. The absence of nucleotide was designed to inhibit dissociation of motors from microtubules; quantification of the number of GFP molecules in mRNPs undergoing motion was precluded by fluctuations in GFP fluorescence intensity and frequent dissociation of RNA:motor complexes from the microtubules. Fluorescein and Cy3 fluorophores were illuminated sequentially for 300 ms and images captured as described above. Cy5-labelled microtubules were imaged at the beginning and end of filming. Solis software (Andor) was used to plot the change over time in fluorescence intensities of Cy3 and GFP signals co-localized on microtubules.

Primary antibodies

Primary antibodies were: rat anti-Dmn (kindly provided by Rahul Warrior[39]; 1:2000 dilution), mouse anti-Dlic (kindly provided by Thomas Hays[40]; 1:3000 dilution), rabbit anti-Egl (kindly provided by Caryn Navarro and Ruth Lehmann[41]; 1:5,000 dilution), mouse anti-BicD 1B11 (kindly provided by Beat Suter[42]; 1:300 dilution) and mouse anti-Dhc 2C11-2 (kindly provided by the Developmental Studies Hybridoma Bank[43]; 1:200 dilution)).

In situ hybridization

DIG or biotin labelled antisense probes were prepared by SP6-mediated *in vitro* transcription from PCR-generated templates using 10x RNA labelling mixes (Roche). *hA* and *hB* corresponded to nucleotides 1291 – 1721 and 1761 – 2193 of the *h* mRNA (Genbank: NM_001014577), respectively.

Fixation, proteinase K treatment and post-fixation of embryos was as described[44]. Hybridization and post-hybridization washes were performed as described[29], with a hybridization temperature of 65°C. Blocking and antibody staining were performed in 20% Western Blocking Reagent (Roche) in PBS with 0.1% Tween-20. Primary antibodies were: mouse anti-biotin (Invitrogen) and sheep anti-DIG (Roche), diluted 1:1000 and 1:500, respectively. Secondary antibodies were: Alexa555 donkey anti-mouse IgG (H + L) and Alexa488 donkey anti-sheep IgG (H + L) (Invitrogen), diluted 1:500. Embryos were mounted in Vectashield with DAPI (Vector Laboratories) and imaged with a 710 confocal microscope (Carl Zeiss) using a Plan Apochromat 63 x/1.4NA oil immersion objective.

For each embryo, two 15 μm x 15 μm images within expression domains were used to give a value for percentage of overlap of the biotin-derived signal with the DIG-derived signal per embryo using manual analysis in Image J (NIH). To control for any systematic errors in the alignment of the signals from red and green channels, *in situ* hybridization experiments always included a set of embryos hybridized with a single *h* 3′UTR antisense probe labelled with both DIG and biotin. According to the manufacturer's instructions, DIG-UTP and biotin-UTP are typically incorporated once per 20 – 25 nt of probe using the procedure employed. Each hapten-bound primary antibody is expected to be bound by multiple polyclonal secondary antibodies and, according to the manufacturers, each Alexa488- or Alexa555-conjugated secondary antibody molecule contains, respectively, ~ 4 or 6 dye molecules. Although the efficiency of antibody binding is likely to be substantially lower than maximal, there is still scope for many fluorophores to be present on a single RNA molecule. Consistent with the ability of the microscope to detect a small number of primary antibodies bound to a puncta containing a single *h* RNA molecule, we were able to detect discrete puncta on the surface of blastoderm nuclei using a Nup214 antibody[45] (a kind gift of Christos Samakovlis) and Alexa-conjugated secondaries. These puncta presumably derive from individual nuclear pore complexes, which are each expected to contain eight copies of the Nup214 protein (Ref. 20 and citations therein).

Statistics

Information on statistical tests is included in the appropriate figure legends.

References

34. Loiseau P, Davies T, Williams LS, Mishima M, Palacios IM. Drosophila PAT1 is required for Kinesin-1 to transport cargo and to maximize its motility. Development. 2010; 137:2763–2772. [PubMed: 20630947]

35. Pandey R, Heeger S, Lehner CF. Rapid effects of acute anoxia on spindle kinetochore interactions activate the mitotic spindle checkpoint. J. Cell Sci. 2007; 120:2807–2818. [PubMed: 17652159]

36. Januschke J, et al. Polar transport in the Drosophila oocyte requires Dynein and Kinesin I cooperation. Curr. Biol. 2002; 12:1971–1981. [PubMed: 12477385]

37. Cole K, Truong V, Barone D, McGall G. Direct labeling of RNA with multiple biotins allows sensitive expression profiling of acute leukemia class predictor genes. Nucleic Acids Res. 2004; 32:e86. [PubMed: 15205470]

38. Ross JL, Shuman H, Holzbaur EL, Goldman YE. Kinesin and dynein-dynactin at intersecting microtubules: motor density affects dynein function. Biophys J. 2008; 94:3115–3125. [PubMed: 18227130]

39. Duncan JE, Warrior R. The cytoplasmic dynein and kinesin motors have interdependent roles in patterning the Drosophila oocyte. Curr. Biol. 2002; 12:1982–1991. [PubMed: 12477386]

40. Mische S, et al. Dynein light intermediate chain: an essential subunit that contributes to spindle checkpoint inactivation. Mol. Biol. Cell. 2008; 19:4918–4929. [PubMed: 18799620]

41. Mach JM, Lehmann R. An Egalitarian-BicaudalD complex is essential for oocyte specification and axis determination in Drosophila. Genes Dev. 1997; 11:423–435. [PubMed: 9042857]

42. Suter B, Steward R. Requirement for phosphorylation and localization of the Bicaudal-D protein in Drosophila oocyte differentiation. Cell. 1991; 67:917–926. [PubMed: 1959135]

43. Sharp DJ, et al. Functional coordination of three mitotic motors in Drosophila embryos. Mol. Biol. Cell. 2000; 11:241–253. [PubMed: 10637305]

44. Lecuyer E, Parthasarathy N, Krause HM. Fluorescent in situ hybridization protocols in Drosophila embryos and tissues. Methods Mol. Biol. 2008; 420:289–302. [PubMed: 18641955]

45. Roth P, et al. The Drosophila nucleoporin DNup88 localizes DNup214 and CRM1 on the nuclear envelope and attenuates NES-mediated nuclear export. J. Cell Biol. 2003; 163:701–706. [PubMed: 14638854]

Supplementary Material

Refer to Web version on PubMed Central for supplementary material.

Acknowledgments

This work was funded by the UK Medical Research Council (project U105178790) and a Lister Institute prize fellowship (to SB). We are very grateful to Andrew Carter, Antoine Guichet, Thomas Hays, Ruth Lehmann, Eric Miska, Caryn Navarro, Isabel Palacios, Jordan Raff, Christos Samakovlis, Beat Suter, and Rahul Warrior for providing reagents, Adam Paré for advice on *in situ* hybridization, Nick Barry for advice on microscopy, Alastair Nicol and Daniel Zicha for help with mRNP tracking software, Marileen Dogterom for the Stepfinder algorithm, and members of the Bullock lab, Daniel St Johnston and Andrew Carter for their valuable insights.

References

1. Holt CE, Bullock SL. Subcellular mRNA localization in animal cells and why it matters. Science. 2009; 326:1212–1216. [PubMed: 19965463]

2. Wilkie GS, Davis I. Drosophila wingless and pair-rule transcripts localize apically by dynein-mediated transport of RNA particles. Cell. 2001; 105:209–219. [PubMed: 11336671]

3. Welte MA, Gross SP, Postner M, Block SM, Wieschaus EF. Developmental regulation of vesicle transport in Drosophila embryos: forces and kinetics. Cell. 1998; 92:547–557. [PubMed: 9491895]

Europe PMC Funders Author Manuscripts

4. Dienstbier M, Boehl F, Li X, Bullock SL. Egalitarian is a selective RNA-binding protein linking mRNA localization signals to the dynein motor. Genes Dev. 2009; 23:1546–1558. [PubMed: 19515976]

5. Navarro C, Puthalakath H, Adams JM, Strasser A, Lehmann R. Egalitarian binds dynein light chain to establish oocyte polarity and maintain oocyte fate. Nat. Cell Biol. 2004; 6:427–435. [PubMed: 15077115]

6. Bullock SL, Ish-Horowicz D. Conserved signals and machinery for RNA transport in Drosophila oogenesis and embryogenesis. Nature. 2001; 414:611–616. [PubMed: 11740552]

7. Hoogenraad CC, et al. Mammalian Golgi-associated Bicaudal-D2 functions in the dynein-dynactin pathway by interacting with these complexes. EMBO J. 2001; 20:4041–4054. [PubMed: 11483508]

8. Bullock SL, Nicol A, Gross SP, Zicha D. Guidance of bidirectional motor complexes by mRNA cargoes through control of dynein number and activity. Curr. Biol. 2006; 16:1447–1452. [PubMed: 16860745]

9. Vendra G, Hamilton RS, Davis I. Dynactin suppresses the retrograde movement of apically localized mRNA in Drosophila blastoderm embryos. RNA. 2007; 13:1860–1867. [PubMed: 17901156]

10. Serano TL, Cohen RS. A small predicted stem-loop structure mediates oocyte localization of Drosophila K10 mRNA. Development. 1995; 121:3809–3818. [PubMed: 8582290]

11. Bullock SL, Ringel I, Ish-Horowicz D, Lukavsky PJ. A'-form RNA helices are required for cytoplasmic mRNA transport in Drosophila. Nat. Struct. Mol. Biol. 2010; 17:703–709. [PubMed: 20473315]

12. Ingham PW, Howard KR, Ish-Horowicz D. Transcriptional pattern of the *Drosophila* segmentation gene hairy. Nature. 1985; 318:439–445.

13. Fusco D, et al. Single mRNA molecules demonstrate probabilistic movement in living mammalian cells. Curr. Biol. 2003; 13:161–167. [PubMed: 12546792]

14. Larsen KS, Xu J, Cermelli S, Shu Z, Gross SP. BicaudalD actively regulates microtubule motor activity in lipid droplet transport. PLoS ONE. 2008; 3:e3763. [PubMed: 19018277]

15. Shubeita GT, et al. Consequences of motor copy number on the intracellular transport of kinesin-1-driven lipid droplets. Cell. 2008; 135:1098–1107. [PubMed: 19070579]

16. Vale RD, et al. Direct observation of single kinesin molecules moving along microtubules. Nature. 1996; 380:451–453. [PubMed: 8602245]

17. Ross JL, Wallace K, Shuman H, Goldman YE, Holzbaur EL. Processive bidirectional motion of dynein-dynactin complexes in vitro. Nat. Cell Biol. 2006; 8:562–570. [PubMed: 16715075]

18. Shu D, Zhang H, Jin J, Guo P. Counting of six pRNAs of phi29 DNA-packaging motor with customized single-molecule dual-view system. EMBO J. 2007; 26:527–537. [PubMed: 17245435]

19. Kardon JR, Reck-Peterson SL, Vale RD. Regulation of the processivity and intracellular localization of Saccharomyces cerevisiae dynein by dynactin. Proc. Natl. Acad. Sci. USA. 2009; 106:5669–5674. [PubMed: 19293377]

20. Schuster M, Lipowsky R, Assmann MA, Lenz P, Steinberg G. Transient binding of dynein controls bidirectional long-range motility of early endosomes. Proc. Natl. Acad. Sci. USA. 2011; 108:3618–3623. [PubMed: 21317367]

21. Coy DL, Hancock WO, Wagenbach M, Howard J. Kinesin's tail domain is an inhibitory regulator of the motor domain. Nat. Cell Biol. 1999; 1:288–292. [PubMed: 10559941]

22. Mallik R, Petrov D, Lex SA, King SJ, Gross SP. Building complexity: an in vitro study of cytoplasmic Dynein with in vivo implications. Curr. Biol. 2005; 15:2075–2085. [PubMed: 16332532]

23. Kiebler MA, Bassell GJ. Neuronal RNA granules: movers and makers. Neuron. 2006; 51:685–690. [PubMed: 16982415]

24. Mhlanga MM, et al. In vivo colocalisation of oskar mRNA and trans-acting proteins revealed by quantitative imaging of the Drosophila oocyte. PLoS ONE. 2009; 4:e6241. [PubMed: 19597554]

25. Delanoue R, Herpers B, Soetaert J, Davis I, Rabouille C. Drosophila Squid/hnRNP helps Dynein switch from a gurken mRNA transport motor to an ultrastructural static anchor in sponge bodies. Dev. Cell. 2007; 13:523–538. [PubMed: 17925228]

Europe PMC Funders Author Manuscripts

26. Lange S, et al. Simultaneous transport of different localized mRNA species revealed by live-cell imaging. Traffic. 2008; 9:1256–1267. [PubMed: 18485054]
27. Ferrandon D, Koch I, Westhof E, Nusslein-Volhard C. RNA-RNA interaction is required for the formation of specific bicoid mRNA 3′ UTR-STAUFEN ribonucleoprotein particles. EMBO J. 1997; 16:1751–1758. [PubMed: 9130719]
28. Pare A, et al. Visualization of individual Scr mRNAs during Drosophila embryogenesis yields evidence for transcriptional bursting. Curr. Biol. 2009; 19:2037–2042. [PubMed: 19931455]
29. Wilkie GS, Shermoen AW, O'Farrell PH, Davis I. Transcribed genes are localized according to chromosomal position within polarized Drosophila embryonic nuclei. Curr. Biol. 1999; 9:1263–1266. [PubMed: 10556096]
30. Nasiadka A, Dietrich BH, Krause HM. Anterior-posterior patterning in the *Drosophila* embryo. Adv. Dev. Biol. Biochem. 2002; 12:155–204.
31. Mikl M, Vendra G, Kiebler MA. Independent localization of MAP2, CaMKIIα and β-actin RNAs in low copy numbers. EMBO Rep. 2011; 12:1077–1084. [PubMed: 21869818]
32. Zimyanin VL, et al. In vivo imaging of oskar mRNA transport reveals the mechanism of posterior localization. Cell. 2008; 134:843–853. [PubMed: 18775316]
33. Kerssemakers JW, et al. Assembly dynamics of microtubules at molecular resolution. Nature. 2006; 442:709–712. [PubMed: 16799566]

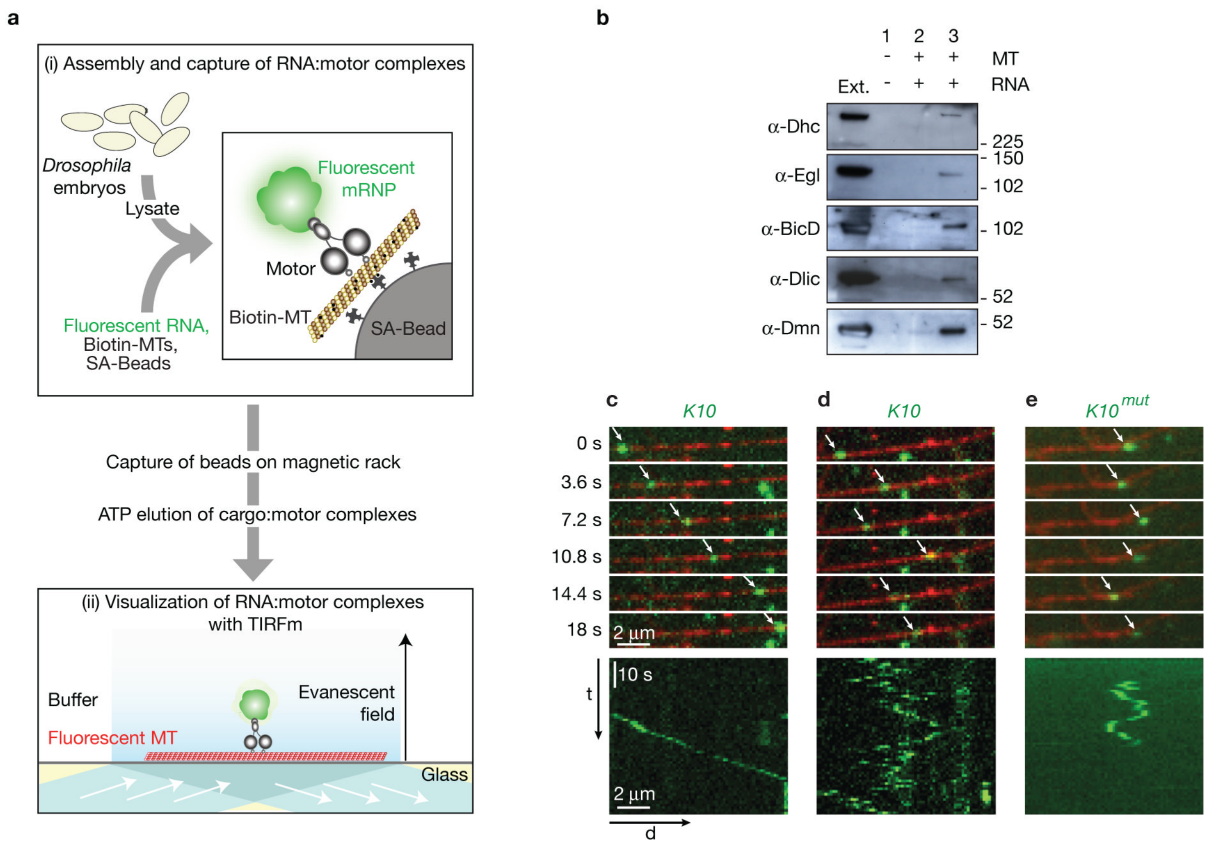

Figure 1. An assay for mRNP motility along single microtubules *in vitro*

(**a**) Schematic of procedure. (i) Full length mRNAs with ~ nine Cy3 dyes per molecule were incubated with embryo extracts in the presence of biotinylated microtubules (MTs) and streptavidin (SA)-conjugated magnetic beads. This allowed the capture of cargo:motor complexes, including those mRNPs containing the fluorescent RNA (inset). (ii) Following brief washing on a magnetic rack, motor complexes were released with ATP and injected into a flow cell containing stable, fluorescein-labelled microtubules, and Cy3-RNA puncta visualized with TIRF microscopy. (**b**) Immunoblots of samples eluted in the presence of ATP following incubation of streptavidin-coated beads with embryo extract alone (lane 1), Cy3-*K10* RNA and embryo extract (lane 2), or Cy3-*K10* RNA, embryo extract and biotinylated microtubules (lane 3). Extract lane (Ext.) represents 2% of the amount added to the streptavidin beads. Dhc and Dlic are the heavy and light intermediate chains of dynein, respectively; Dmn is Dynamitin (a dynactin sub-unit). Positions of molecular weight markers are shown. Original scans of the blots are shown in supplementary figure 6. (**c–e**) Stills (upper panels) and kymographs (lower panels) generated from time-lapse series of motile *K10* (**c**, **d**) and *K10*^{mut} mRNPs (**e**). **c** shows unidirectional motion; **d** and **e** show bidirectional motion (these data are derived from Supplementary movies S2 and S3, respectively). Images are pseudocoloured for clarity (green, Cy3 signal; red, fluorescein-labelled microtubule). Arrows, position of motile mRNP; t, time; d, distance. It should be noted that only ~ 10% of microtubule-associated puncta of both mRNA species moved during the 3 minutes of imaging. Essential regulatory components were presumably lost

Europe PMC Funders Author Manuscripts

from many RNA:motor complexes during their capture from embryos, or their motor activity compromized.

Europe PMC Funders Author Manuscripts

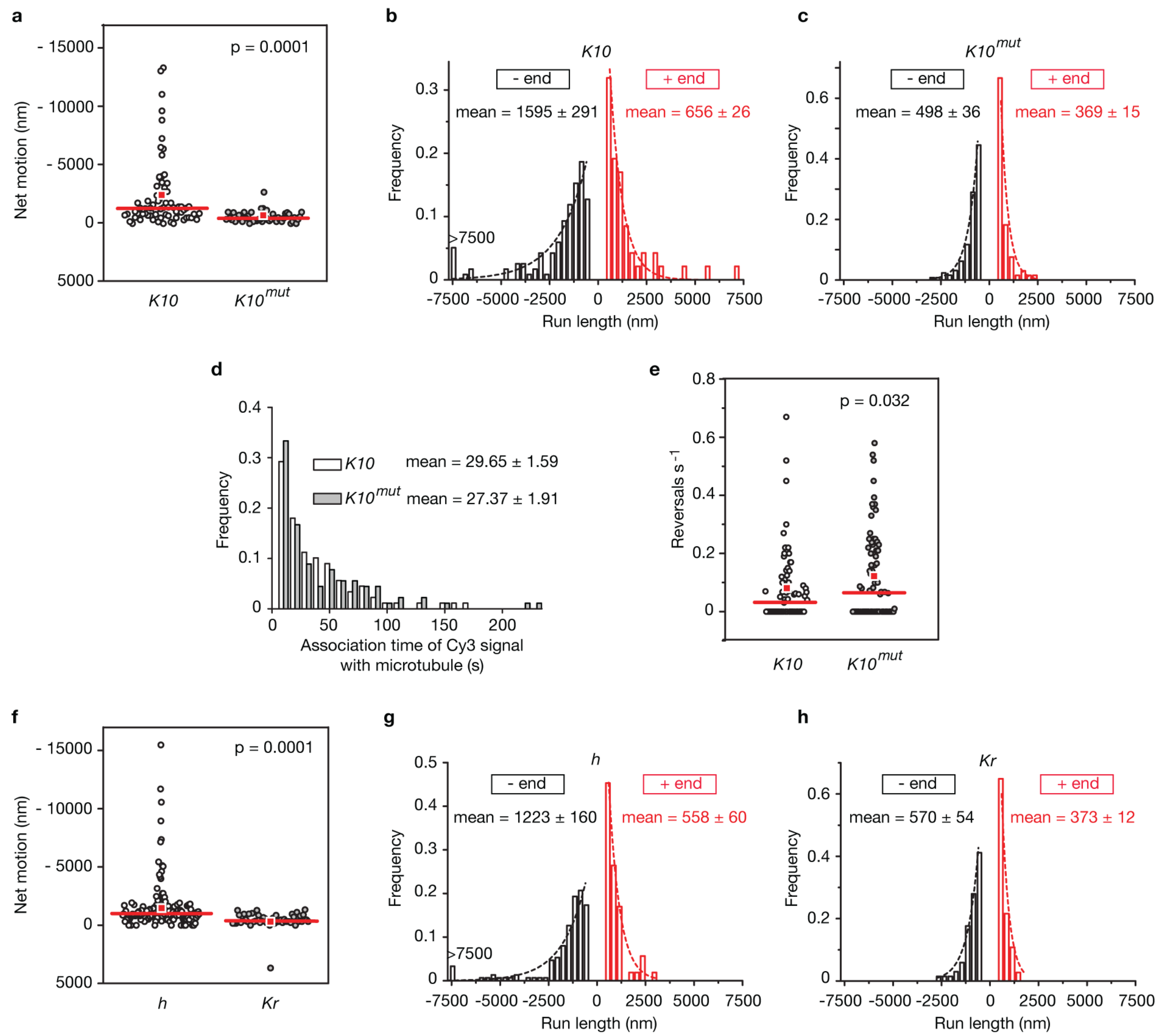

Figure 2. Differential motility of localizing and non-localizing mRNPs along polarity-marked microtubules *in vitro*

(**a**–**c**) Quantification of net RNA motion (**a**; negative values are net minus-end-directed movement) and lengths of minus-end- and plus-end-directed runs (**b**, **c**) of motile *K10* and *K10^{mut}* mRNPs. A run was defined as a persistent movement in either the minus-end or plus-end direction with a total length ≥ 320 nm (≥ 2 pixels) that was ended with either a reversal in the direction of movement of the mRNP or disappearance of the Cy3 signal (presumably due to a dissociation event or photobleaching). (**d**, **e**) Association times of Cy3 signals with microtubules (**d**) and reversal frequencies (**e**) for motile *K10* and *K10^{mut}* mRNPs. (**f**–**h**) Quantification of net RNA motion (**f**) and lengths of minus-end- and plus-end-directed runs (**g**, **h**) of motile *h* and *Kr* mRNPs. In **a**, **e** and **f**, red horizontal lines and squares represent, respectively, median, and mean values. In **b**, **c**, **g** and **h**, mean run lengths were calculated from decaying exponential distributions fitted to the data (dashed lines). Run lengths were significantly greater in the minus-end than the plus-end direction for all

RNAs (Mann Whitney test; *K10* and *K10^{mut}*, p = 0.001; *h*, p <0.0001; *Kr*, p = 0.02). Numbers of motile mRNPs analyzed were: *K10*, 98; *K10^{mut}*, 89; *h*, 131; *Kr*, 55. All errors are shown as s.e.m..

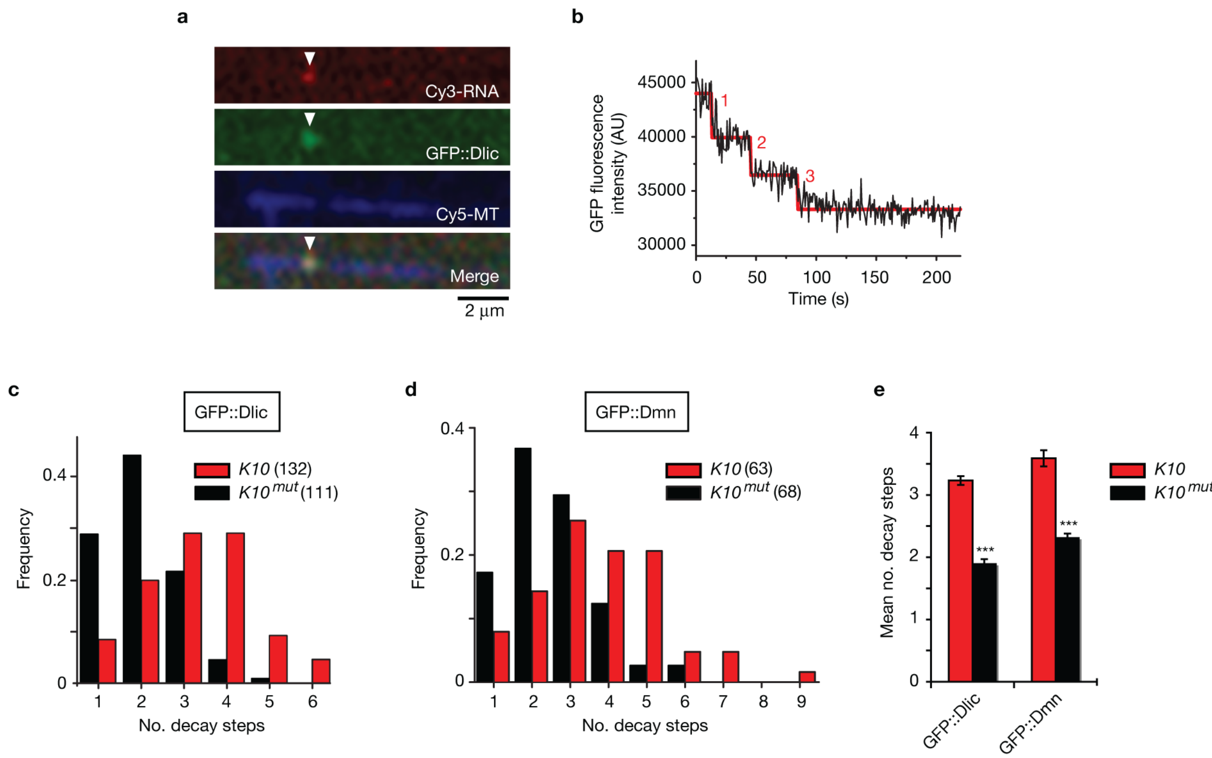

Figure 3. Localizing mRNPs contain, on average, more copies of dynein and dynactin components than non-localizing mRNPs

(**a**) Example of co-localization of Cy3-*K10* RNA and GFP::Dlic immobilized on a microtubule *in vitro*. (**b**) Example of three-step photobleaching of GFP signal (from a microtubule-associated Cy3-*K10* mRNP associated with GFP::Dlic) before reaching the baseline level of fluorescence in the chamber (red line shows output of the step-fitting algorithm Stepfinder[33]; predicted bleaching steps are shown by red numbers). See Supplementary figure 3a for additional examples of traces. Varying the frequency of illumination with the 488-nm laser demonstrated that the decay in the GFP signal over time was indeed a function of photobleaching of stably associated proteins (Supplementary Fig. S3b). (**c**, **d**) Distribution of GFP decay steps exhibited by the population of mRNPs from GFP::Dlic (**c**) or GFP::Dmn (**d**) extracts associated with *K10* or *K10^{mut}* RNA and microtubules. Data were generated from manual analysis of the raw traces, although very similar results were obtained with the Stepfinder algorithm[33] and with manual analysis of data that was denoised with a moving average. Number of mRNPs analyzed are shown in parentheses. We assume that localization signals recruited additional copies of the intact dynein-dynactin complex to a sizeable subset to mRNPs; a substantial proportion of the unlabelled, endogenous Dlic or Dmn in the extracts (Supplementary Fig. S3d) means that discrete peaks in the distribution of GFP::Dlic or GFP::Dmn decay steps would not be observed with the number of complexes that could be practically analyzed. (**e**) Mean number of GFP decay steps (± s.e.m.) from **d** and **e** (calculated from fitting a Gaussian distribution, including the predicted contributions of mRNPs that contain only unlabelled copies of the protein). ***, $p < 0.001$ (t-test), compared to number of GFP decay steps of *K10* mRNPs.

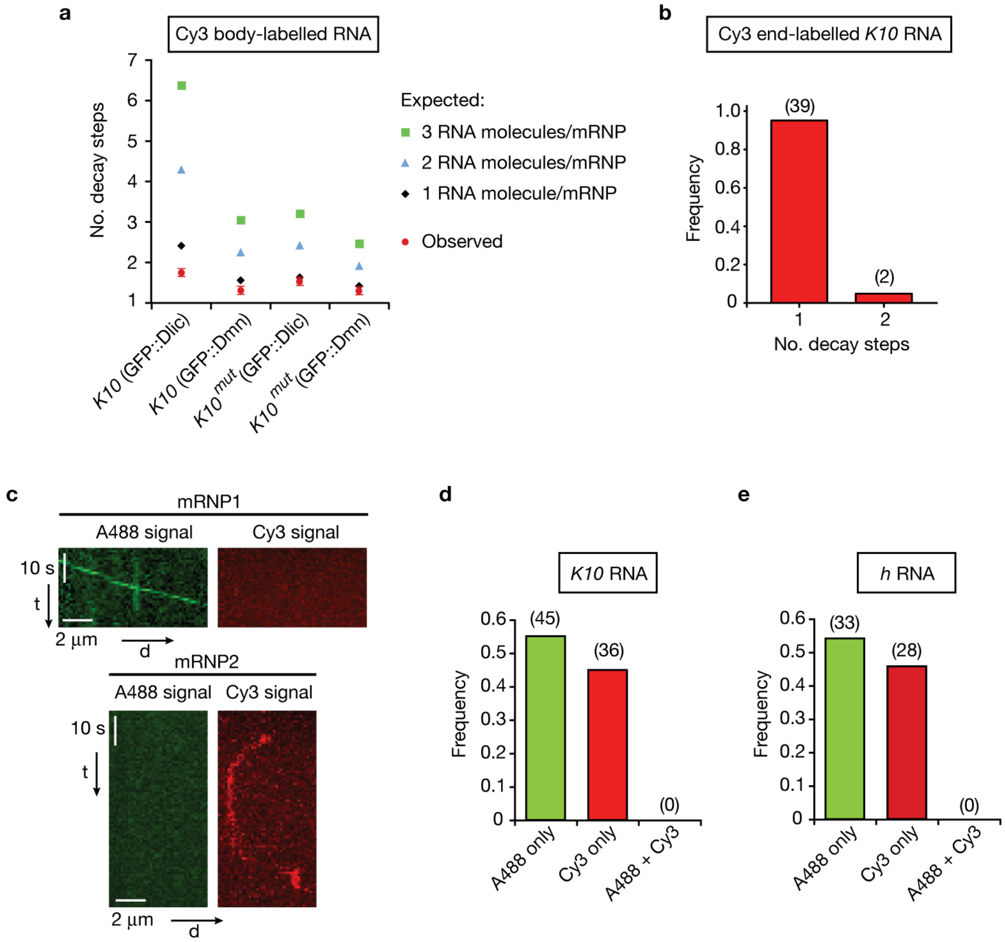

Figure 4. Single copies of mRNA molecules within the majority of localizing mRNPs *in vitro*

(**a**) Comparison of the observed values for mean number of Cy3 decay steps of mRNPs containing body-labelled RNA (and associated with Cy5-microtubules and the protein indicated in parentheses), with the values expected for one, two or three RNA molecules per mRNP. Expected values were calculated based on the number of Cy3 molecules per RNA molecule in each body-labelled RNA preparation (Supplementary Fig. S4). The calculation assumed a Poisson distribution of Cy3 incorporation per RNA and considered that the proportion of RNA molecules without a Cy3 dye would not be visible in an experiment. For observed values, number of mRNPs analyzed were: *K10* (GFP::Dlic), 44; *K10* (GFP::Dmn), 53; $K10^{mut}$ (GFP::Dlic), 49; $K10^{mut}$ (GFP::Dmn), 35. Observed mean values are slightly lower than the expected mean values for a single RNA molecule per mRNP, presumably due to a fraction of fluorophores that bleach before data capture commences or are non-energizable[18, 19]. (**b**) Observed number of decay steps exhibited by mRNPs containing *K10* RNA subjected to a 3′ end-labelling reaction with Cy3 and associated with signals from GFP::Dlic and Cy5-microtubules *in vitro*. In this and other panels the numbers of mRNPs observed in each category are shown in parentheses. Given the degree of labelling in the RNA population (0.59 Cy3 dyes per RNA molecule), the number of decay steps observed is significantly different from that expected from two *K10* RNA molecules per mRNP (p

<0.0001) or an equal proportion of mRNPs containing one and two *K10* molecules ($p<0.05$) (χ^2 test). (**c**) Kymographs of representative motile *K10* mRNPs assembled in the presence of equimolar Alexa-488 (A488)-labelled RNA and Cy3-labelled RNA. Signals were detected either from A488 (left panels) or Cy3 (right panels), but not both. t, time; d, distance. (**d** and **e**) Quantification of the fluorescent signal displayed by motile mRNPs assembled in the presence of both A488-*K10* and Cy3-*K10* (**d**) or both A488-*h* and Cy3-*h* (**e**). All errors are shown as s.e.m..

Europe PMC Funders Author Manuscripts

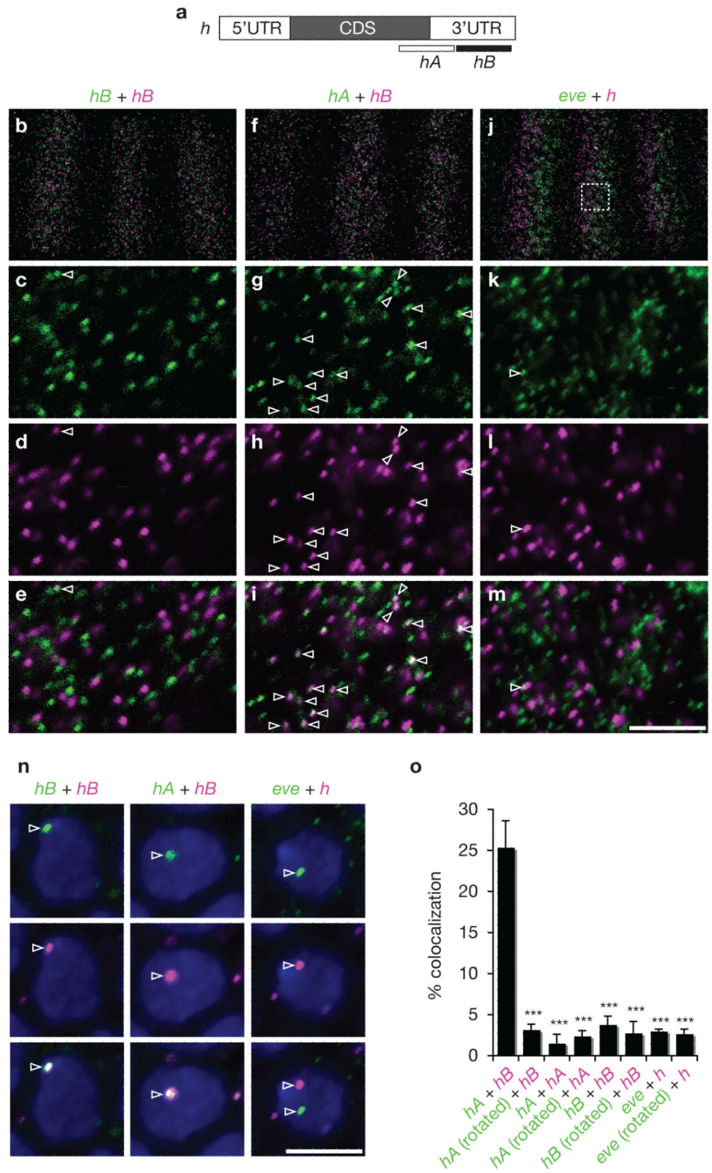

Figure 5. Single copies of an RNA species within the majority of apically localized mRNPs *in vivo*
(**a**) Schematic of the full-length *h* mRNA and *hA* and *hB* antisense probes (CDS, coding sequence; UTR, untranslated region). (**b**, **f** and **j**) Low power images of *Drosophila* embryos hybridized with the indicated probe sets, demonstrating specific detection of the RNAs (which are transcribed in stripes[30]). Signals shown in green derive from DIG probes detected with sheep anti-DIG and Alexa488-anti-sheep antibodies. Those shown in magenta derive from biotin probes detected with mouse anti-biotin and Alexa555-anti-mouse antibodies. Dashed box in **j** shows region containing many puncta of *h* and *eve*, typical of areas imaged at higher magnification for co-localization assays. (**c**–**e**, **g**–**i** and **k**–**m**) High-

Europe PMC Funders Author Manuscripts

magnification, grazing confocal images of the apical cytoplasm. Frequent co-localization is seen between *hA* and *hB* signals (**g–i**), but not between *hB* and *hB* probes labelled with different haptens (**c–e**) or *h* and *eve* (**k–m**) (note that significant co-localization was also not observed for *hA* and *hA* probes labelled with different haptens (see **o**)). Arrowheads indicate examples of co-localized signals (for clarity, not all examples are labelled in **g–i**). (**n**) Detection of nascent transcript foci (arrowheads) by the indicated probe sets. DAPI, blue. Note distinct sites of transcription for *h* and *eve*. (**o**) Quantification of co-localization percentages. Y-axis indicates mean percentage of biotin probe-derived signals that co-localized with a DIG-derived probe signal; error bars are s.e.m. (n = 6 embryos per experimental condition). 'Rotated' refers to the control simulating a random distribution of dots by rotating the image of each DIG probe-derived signal by 90° and overlaying it on the original biotin probe-derived image. ***, $p < 0.001$ (t-test), compared to percentage co-localization of *hA* and *hB* signals. Scale bars in **m** and **n** represent 35 μm in **b**, **f** and **j** and 5 μm in other panels.